ADVANCED MATERIALS INTERFACES
Open Access
www.advmatinterfaces.de

Interfacial Yield Stress Response in Synthetic Mucin Solutions

*Sumit Sunil Kumar, Travis Leadbetter, J. Brandon McClimon, Manuel A. Lema, Farhana M. Khan, Prashant K. Purohit, Adam B. Braunschweig, and Robert W. Carpick**

The solution rheology of a fully synthetic, monodisperse mucin that mimics the glycosylated domains of natural mucins, poly(β-Gal-Thr)$_{22}$, is studied to systematically explore relationships between polymer structure, solution conditions, and rheological properties. Using standard cone-plate rheometry, shear thinning is observed over a range of concentrations, with an apparent yield stress—typical for gels—evident at the highest concentrations. This is surprising given the dilute, weakly interacting nature of the solutions and the lack of observable structure in cryogenic electron microscopy and particle tracking microrheology. However, interfacial rheometry demonstrates that the gel-like behavior is attributable to a thin structured layer at the air–water interface, without any bulk gelation. This is attributed to an interfacial layer formed by inter-mucin H-bonds that yields when sheared. A computational model using kinetic Monte Carlo (kMC) simulations qualitatively reproduces the yield stress response of such a network through an intermolecular bonding potential. An analytical model of stochastic bond formation and breaking, validated by the kMC simulations, demonstrates that having multiple bonding sites per mucin with a force-dependent debonding rate aligns with experiments, consistent with intermolecular interactions for other mucin proteins. This suggests that in mucin solutions, gelation may begin at the air–water interface, and emphasizes the need for multitechnique validation when exploring structural cues of mucus gelation through rheometry.

1. Introduction

Secreted mucus hydrogels are deployed by all animals[1] to provide protection,[2] lubrication[3] and adhesion[4] at biological interfaces.[1,5–9] For example, in the respiratory tract, epithelial cells secrete mucus, creating a protective barrier, with cilia assisting in transporting the mucus from the lungs to the throat for the removal of harmful particles from the lungs.[10] While mechanistic details of mucociliary clearance are still debated, it is broadly agreed that mucus elasticity permits the cilia to transfer momentum to the mucus layer.[11] A shear thinning response, in particular, facilitates rapid mucus clearance by coughing since under rest the mucus lining remains unperturbed, but when it accumulates, coughing makes removing mucus easier since the viscosity decreases at high shear rates, which is driven by rapidly moving air over the mucus. Moreover, mucus dysfunction underlies various health complications. For instance, a change in a mucus' rheological properties affects

S. S. Kumar, J. B. McClimon, P. K. Purohit, R. W. Carpick
Department of Mechanical Engineering and Applied Mechanics
University of Pennsylvania
Philadelphia, PA 19104, USA
E-mail: carpick@seas.upenn.edu

T. Leadbetter
Graduate Group in Applied Mathematics and Computational Science
University of Pennsylvania
Philadelphia, PA 19104, USA

M. A. Lema, F. M. Khan, A. B. Braunschweig
Advanced Science Research Center
Graduate Center at the City University of New York
New York, NY 10031, USA

M. A. Lema, F. M. Khan, A. B. Braunschweig
Department of Chemistry
Hunter College
New York, NY 10065, USA

M. A. Lema, A. B. Braunschweig
PhD Program in Chemistry
Graduate Center at the City University of New York
New York, NY 10016, USA

M. A. Lema, F. M. Khan, A. B. Braunschweig
Nomi Materials Corp.
New York, NY 10040, USA

A. B. Braunschweig
PhD Program in Biochemistry
Graduate Center at the City University of New York
New York, NY 10016, USA

The ORCID identification number(s) for the author(s) of this article can be found under https://doi.org/10.1002/admi.202500066

DOI: 10.1002/admi.202500066

its shear thinning behavior, making it either too difficult to remove at high speeds or not viscous enough at equilibrium to act as an effective protective layer. These mechanisms have been implicated in the causes of cystic fibrosis[12] and dry-eye disease.[13] There are many other conditions in which mucus has a role in progression, but little is known about how mucus viscoelasticity may contribute.

Both the relationship to human health and the desire to capitalize on synthetic materials that recreate the properties of their natural counterparts motivate fundamental studies of the rheological properties of mucus. However, challenges related to heterogeneity, stability, and the ability to obtain samples in sufficient quantity for systematic study have significantly hampered the understanding of these essential biomaterials. The structure and properties of mammalian mucus are primarily attributed to mucin proteins.[14] Mucins are typically high molecular weight (1–10 MDa) proteins, with highly *O*-glycosylated domains and terminal, cysteine-rich domains.[1] Bonding between mucins is purported to occur through disulfide crosslinking, H-bonding between glycans, and Ca^{2+}-mediated ionic bridging between glycans, making the viscoelastic response of mucus variable and sensitive to reducing conditions, pH, and ionic strength.[15] Moreover, the mucus hydrogels themselves are heterogenous mixtures, consisting of multiple different mucins along with other proteins, enzymes, glycans, and lipids. To address this, rheological and tribological studies have been performed with purified mucin proteins. However, purification often degrades the mucins,[16] changing measured viscosity, lubricity,[17] and adhesion.[18,19] An alternate approach to extract mucin features involves using mucus collected from epithelial cell cultures, reducing the contamination issue.[20] However, whether extracted from live species or cultured, natural mucus often contains a variety of mucins (e.g., MUC2, MUC5) which have different chemical compositions, chain lengths, and molecular weights,[21] as well as other proteins, ions, and cellular materials, and this polydispersity complicates the mechanistic study of their properties.[22] To address these challenges, there is a need to study the viscoelastic properties of synthetic analogues of mucus whose structures mimic those of natural mucins, are easily tuned so that structure-activity relationships can be explored systematically, and that can be prepared in sufficient quantity. In addition to the insights into human health, the data from such studies could also inform the design of biomimetic materials as adhesive, lubricants, and semi-permeable barriers for mediating interactions at biotic/biotic or biotic/abiotic interfaces.

Synthetic mucins,[23,24] which are synthetic polymers designed to mimic the structures and properties of their natural counterparts have a large array of existing and future potential applications including skincare and cosmetics,[25] drug delivery,[26–28] tissue engineering, surgical implant coatings,[29] cartilage lubrication,[30] and antimicrobial coatings.[31] These polymers offer uniquely useful model systems for exploring and understanding the rheological properties of mucuses. Prior studies of synthetic mucin solutions typically show shear thinning and gelation.[32–34] While these synthetic mucins reproduce some rheological properties of natural mucins, synthetic mucins reported to date do not reproduce the chemical structures of natural mucins, particularly as they have non-natural backbones or lack the essential *O*-glycans.[35] As such, the relationship between these studies and how they inform the behavior of natural mucuses is not fully understood,[36] and there remains a pressing need to understand the material (and in this case rheological) properties of mucus using analogues that replicate salient features of their natural counterparts. To this end, herein we report rheological measurements of solutions of monodisperse scalable synthetic mucins which replicate the highly glycosylated domains of natural mammalian mucins.[23] The repeating unit of the synthetic mucin, Gal-Thr, is composed of the amino acid threonine (Thr), which is *O*-glycosylated with the monosaccharide *β*-Galactose (*β*-Gal) to form a chain with average length of 22 units, with one *β*-Gal on every residue, resulting in the polymer, poly(Gal-Thr)$_{22}$.[23,24,35] This polymer mimics the highly glycosylated domains of mammalian mucins, where the great majority of *O*-glycans are Gal-terminated[1] and sandwiched between cysteine-rich domains.[1] The short chain length of these mucins (≈10 nm) renders their backbones effectively rigid due to the steric constraints of the bulky *O*-glycans, simplifying the modeling and interpretation of the experimental results by largely removing effects like chain flexibility, entropic contributions, and chain entanglements. Moreover, as these mucins do not possess any cysteine-containing domains, and solutions with pure water are used, only van der Waals interactions and H-bonding between mucins exist. Thus, rheological studies of this pure, ideal polymer can rationally inform how these domains contribute to the solution rheology of more complex natural mucin.[1,9,37–39] In particular, the common thread in most past mucin solution research is their shear-thinning behavior and their ability to form gels when left undisturbed, due to polymer aggregation, presumably because of cross-links. We examine whether such behavior occurs in this simple, pure synthetic mucus. Through a thorough analysis we reveal that an apparent bulk rheological response matching prior mucin research is in fact due to an interfacial effect, indicating that mucins segregate to the air–water interface. We probe the microphysics of this interfacial layer to further understand the nature of bonding and yielding in this system.

2. Results and Discussion

2.1. Apparent Bulk Rheological Response of Poly(Gal-Thr)$_{22}$ Solutions

Poly(Gal-Thr)$_{22}$ was prepared by polymerization of an *N*-carboxyanhydride monomer *N*-functionalized with acetate-protected *β*-Gal under conditions reported previously,[23] to provide the pure polymer with a M_n = 5800 g mol^{-1} and polydispersity index ($Đ$) = 1.04. The scalability of this approach was critical for this study, as appreciable amounts of mucin were required to conduct the comprehensive set of measurements reported. The rheological response of poly(Gal-Thr)$_{22}$ was studied at different concentrations (0.1, 1, 5, 10 mg mL^{-1}) in deionized (DI) water using rheometry. Like the vast majority of prior work and as is standard in rheometry, we first use a cone-plate rheometer for its key advantage of applying a uniform shear rate to the entire sample. We use lightweight, high diameter Al plates to render inertial effects negligible. Combined with the high sensitivity of the rheometer (TA Instruments, DHR-3), we can reliably measure viscosities at the level of water (0.001 Pa s). See Experimental section for more information.

The dynamic viscosity versus shear rate for all four concentrations (**Figure 1a**) show an extended shear thinning response. Each curve plateaus at high shear rates, where the Newtonian plateau of the water solvent is encountered. The slopes at lower shear rates in Figure 1a provide the shear-thinning exponent. The slopes of the two highest concentrations are indistinguishable: -0.98 ± 0.02 and -0.99 ± 0.03 for 5 and 10 mg mL^{-1}, respectively, while slopes of -0.67 ± 0.06 and -0.67 ± 0.03 were found for 0.1 and 1 mg mL^{-1}, respectively, both of which were close to the experimental noise floor of the device obtained when measuring pure DI water (comparison with DI water is presented in Figure S13a in the Supporting Information). The slopes for the higher concentrations are in agreement with literature on natural mucins, where shear thinning exponents were reported to be in the vicinity of –1,[34,40] though some other literature reports lower shear thinning exponents.[41] These results confirm that poly(Gal-Thr)$_{22}$ possesses a shear thinning response characteristic of natural mucins and other associative polymers.[42–44]

Notably, no plateau at low shear rates is observed, even though a low shear rate plateau is common across many viscoelastic solutions.[33,45] For all concentrations, the viscosity steadily increases to the lowest measured shear rate of 0.1 s^{-1} with decreasing shear rate. The lack of a plateau and a shear thinning exponent of –1 (attained for the two highest concentrations) is characteristic of a fluid exhibiting yield stress behavior,[11,46–48] i.e., a material having a solid-like response at low shear rates (the constant slope of -1 means the shear stress is constant in the low shear region) due to the presence of some type of stabilizing structure like a gel, and a fluid-like response at higher shear rates due to the shear stress breaking up that structure. This feature of mucus would indicate the ability to trap particles and pathogens at low flow rates, while being able to transport them via flow at high shear rates (like in coughing). It has also been discussed as a valuable feature for snail locomotion.[49]

The above observations are consistent with the bulk structural response reported for natural mucin solutions, as intermolecular associations are exhibited by natural mucins and other associative polymers,[33,45,50] albeit typically at lower pH values.[51] Some of these experimental methods have also been interpreted to indicate gelation occurring in cultured natural mucus.[20] This is known to occur in nature. For example, the gelled mucus lining of the stomach serves as a protective barrier when hydrochloric acid or digestive enzymes are secreted during digestion.[32] Thus, it would seem natural to interpret the cone-plate rheometry measurements as showing that solutions of poly(Gal-Thr)$_{22}$ capture key characteristic features of the rheological properties of natural mucus, namely shear thinning and yield stress behavior, which is attributed to interpolymer crosslinking or localized aggregation.[40,52]

However, in cone-plate rheometry, the response of the air–water interface can affect the measurements.[53,54] Thus, we conducted additional measurements to separately analyze the bulk and interfacial responses. To ascertain if bulk structural features are responsible for the observed behavior, cryo-transmission electron microscopy (cryo-TEM) and flow sweeps using a Couette cell geometry were performed.

Previous work on linear molecules, including mucins, has demonstrated that cryo-TEM images can provide unambiguous detail about molecular associations and any resulting extended

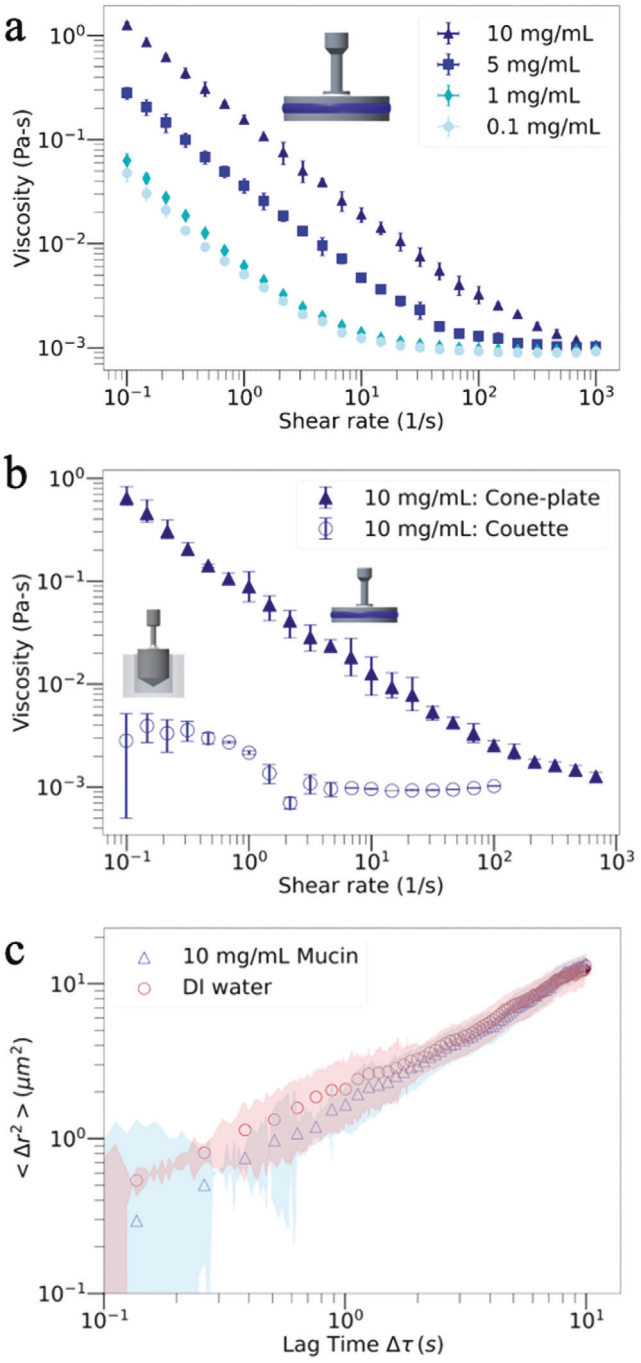

Figure 1. Tests to ascertain bulk polymeric structure. a) Viscosity versus shear rate at four concentrations of poly(Gal-Thr)$_{22}$ in DI water measured by cone-plate rheometry, which probes the bulk and air–water interfacial response. b) Comparison of the cone-plate tests with a Couette cell geometry, which only probes the bulk response. b,c) The data and error bars are the mean and standard deviation of three replicates. c) Particle tracking microrheology measurements, which track the local response within the bulk of the solution, showing the mean squared displacement $\langle \Delta r^2 \rangle$ as a function of lag time for 1 μm fluorescent polystyrene particles suspended in either DI water or 10 mg mL^{-1} synthetic mucin solution. Each dataset is an average of all particle tracks combined from three different videos acquired from different regions of each sample. Logarithmic standard deviation envelopes and best fits using a power law are shown.

structure within the bulk.[52] However, we observed no evidence of extended structure in cryo-TEM (see Figure S2 in the Supporting Information).

Steady shear flow sweeps were then performed using a Couette cell where, unlike the cone-plate rheometer, there is a negligible air–water interface. Thus, the contribution from the bulk fluid dominates the rheological response. The Couette flow sweep data were indistinguishable from the noise floor of the rheometer at all concentrations in the apparent shear thinning regions, implying the solutions have a bulk shear-rate dependent viscosity well below that measured by cone-plate rheometry. As shown in Figure 1b, at 10^{-1} s^{-1}, the bulk viscosity measured in the Couette cell is ≈0.003 Pa s, whereas in the cone-plate geometry the corresponding measured viscosity was two orders of magnitude higher at 0.7 Pa s, confirming the lack of bulk structure.

To further explore the bulk response, particle tracking microrheology[55] was conducted using single fluorescent particles at the highest concentration of 10 mg mL^{-1} mucin and for DI water. The mucin solution shows a Newtonian response indistinguishable from DI water as shown in Figure 1c, highlighted by the linear trend of the mean squared displacements with respect to time as opposed to the strong shear thinning seen in cone-plate measurements (see Section S2 in the Supporting Information for more details). It should be noted that the apparent differences in the mean squared displacements (MSDs) at low lag times are within the margin of error and cannot be confidently attributed to effects such as intermolecular interactions.

The main inference from the cryo-TEM, Couette cell rheometry, and particle tracking micro-rheology is that the cone-plate measurements (Figure 1a) are not reflective of the bulk properties of the mucin solution. We propose instead that the apparent yield stress is due to air–water interfacial effects. This interpretation is motivated by reports of enhanced viscosities, elastic response, and yield-stress like behavior arising from structuring at the air–water interface reported in the rheology of some biological fluids.[53,54]

2.2. Interfacial Rheology behind the Apparent Yield Stress Fluid Response

To examine the interfacial rheology of the mucin solutions directly, interfacial rheometry was performed with a double wall ring geometry (DWR).[56] This constrains the imposed shear to the vicinity of the air–water interface, mitigating effects associated with bulk response. Initial amplitude sweeps were performed for the 10 mg mL^{-1} mucin poly(Gal-Thr)$_{22}$ solution to determine an appropriate strain magnitude for subsequent frequency-dependent oscillatory shear tests. An iterative subphase correction algorithm[57] was used to obtain the correct components of the viscosity and elasticity associated with the interface, and the corrected moduli are shown in **Figure 2**.

At small strain amplitudes (0.001%–1%), the storage modulus exceeds the loss modulus, indicating that gelation has occurred in the interfacial region being probed. Control tests using pure DI water confirm that the measured moduli in Figure 2 are above the experimental noise floor. At higher strain amplitudes (1%–10%) there is first a decrease in the storage modulus, which marks the limit of the linear elastic response.[58] Then there is a crossover

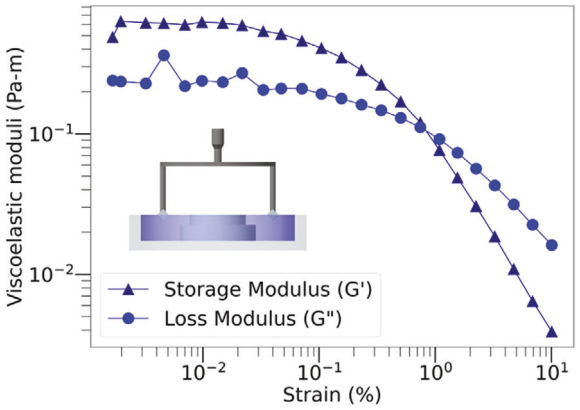

Figure 2. Interfacial rheology of 10 mg mL^{-1} mucin and the predicted structural dynamics using the double walled ring geometry. Amplitude sweeps with an oscillation frequency of 0.1 Hz. These data points are mean values from the replicates passed through the subphase correction algorithm[57] to eliminate bulk fluid effects.

of the storage and loss modulus, which is typical of viscoelastic gels upon exceeding the yield stress[59] This confirms that there is some structuring at the air–water interface, consistent with our hypothesis that the mechanistic response of the solution at the air–water interface is contributing to the cone-plate rheometry measurements.

With knowledge of interfacial structuring in hand, further insight can be gained from the cone-plate results. The corresponding apparent shear stresses for the viscosities shown in Figure 1a are presented in **Figure 3**a. The bulk solution viscosity ascertained from the microparticle tracking measurements (which was indistinguishable from water) are used to subtract the bulk mucin solution contribution to the measured shear stresses. This leaves the component of shear stress which can be attributed to the structured air–water interface. This corrected result shows that the constant interfacial shear stress extends across the entire range of shear stresses for the two highest concentrations (10 and 5 mg mL^{-1})and all but the highest decade of shear rates for the two lower mucin concentrations (1 and 0.1 mg mL^{-1}). To check if the apparent yield stress vanishes when lower shear rates are sampled,[60] another set of tests were performed using the 10 mg mL^{-1} sample, with shear rates resolved to two orders of magnitude lower (to 1.06×10^{-4} s^{-1}). A conclusive yield stress-like response is still observed (see Figure S1, Supporting Information).

The yield stress of 0.11 Pa in the low shear rate limit at 10 mg mL^{-1} is rather low, and even lower and anomalous yield stresses are seen for the lower concentrations. For comparison, for human mucus samples obtained from human bronchial epithelial cell cultures[20] with a far lower measured protein concentration (1.4–1.5 vs 10 mg mL^{-1} in our case), yield stresses of 0.05–0.2 Pa were observed. A thick slug mucus was measured to have a yield stress of 300 Pa,[61] and another had 200 Pa.[62]

In rheometry, it can be difficult with flow sweeps to reach steady state at low shear rates due to the need to acquire data over long timescales, especially for such low shear stress values.[60] Stress-controlled creep tests, where a steady shear stress is imposed and the global fluid response measured, mitigates this problem.[63] We thus conducted creep tests using the cone-plate

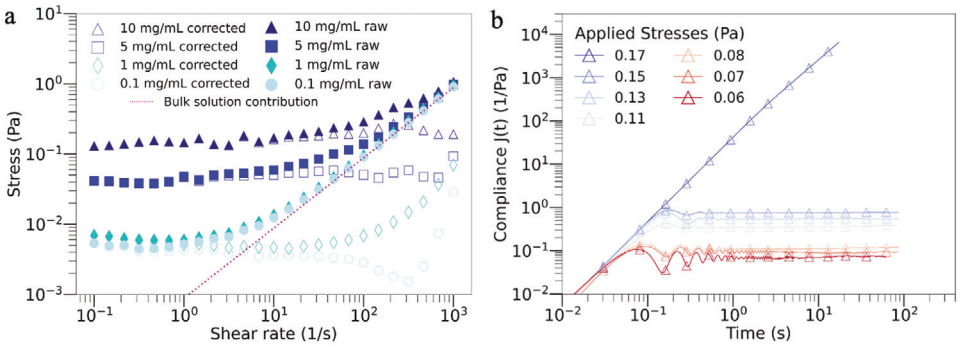

Figure 3. Presence of an apparent yield stress due to interfacial structuring. a) Closed symbols: data extrapolated from (a); open symbols: corrected data after subtracting the bulk solution contribution (pink dashed line). The correct data shows an apparent yield stress at low shear rates, which is concentration dependent. Anomalous stresses at higher shear rates for the two lower concentrations are due to reaching the noise limits of the rheometer. b) Creep tests showing the mucin solution compliance as a function of time with different applied stresses, and close to the yield stress measured in (b) (concentration: 10 mg mL^{-1} poly(Gal-Thr)$_{22}$ in DI water).

rheometer to investigate the apparent yield stress behavior seen at low shear rates in the flow sweeps. These tests were performed with the 10 mg mL^{-1} concentration sample. As shown in Figure 3b, after the initial shear loading phase and brief ringing (associated with the shear load feedback circuit), the compliance for all but the highest shear stress remains approximately constant for the duration of each test. The nearly constant compliance with time indicates that the response is predominantly elastic with little creep, albeit with some non-linear response across this stress range given the increase in steady-state compliance with imposed stress. However, with the highest stress used (0.17 Pa), the fluid yields immediately leading to flow, i.e., the shear stress was sufficient to break up the preexisting fluid microstructure. This value modestly exceeds the apparent yield stress of the fluid in this test (0.11 Pa) and the yield stress measured at even lower shear rates (0.02 Pa) (see Figure S1, Supporting Information). Note that the stress required for yield in the creep tests can be significantly higher than that in the flow curves, due largely to the formation of structure prior to the creep tests – an effect which is absent in the dynamic flow sweeps that constantly break up fluid structure.

Given the apparent yield stress observed while conducting cone-plate rheometry coupled with the interfacial effects observed independently, a comparison of the responses is warranted. The modulus captured in the DWR corresponding to the yield stress in Figure 2 (the crossover point) is 0.1 Pa m, and the yield strain is 0.7%. From the 70 mm diameter of the ring, this corresponds to a force per unit length corresponding to the yield stress at the interface of 7×10^{-4} N m^{-1}. This then gives the force experienced by the DWR along its circumference as 1.54×10^{-4} N at the yield stress. Applying the same force for the air–water interface present in the 60 mm diameter cone-plate geometry gives an expected torque of 4.61 μN m. The torque in the cone plate experiment corresponding to the apparent yield stress in Figure 3 is 0.3 ± 0.04 μN m. Thus, the measured yield stress of the interface from the DWR can more than fully account for the torque measured in the cone-plate geometry; the difference in these two values may be due to different interfacial structures, or experimental uncertainty. Regardless, we conclude that air–water interfacial behavior dominates the cone-plate measurements and is responsible for the yield stress behavior, which is strong even at long time scales, as shown by the elastic response in the creep tests, indicating that intermolecular associations and solid-like structuring do happen with the mucins, but these responses are dominant at the air–water interface.

The origin of this interfacial structuring is surprising as prior mucin literature reports yield stress behavior and attributes it to bulk structuring.[18,33,34,45] However, recent work on the structural dynamics of natural mucins that went beyond cone-plate rheometry showed the possibility of interfacial effects dominating over bulk effects. For example, a weak but nonetheless gel-like interfacial response was reported for bovine submaxillary mucins (BSM).[64] In another recent report, in this case for mucus from cultured human bronchial epithelium cells (thus avoiding challenges with contamination from in vivo samples), macroscopic cone-plate rheometry was consistent with yield-stress behavior, while micro-rheology using optical tweezer-controlled microparticles revealed Newtonian water-like behavior. The authors attributed this to heterogeneity within the mucus, assuming that the microparticles were moving within Newtonian liquid within pores of a network of stiffer gel-like filaments.[20] However, the authors noted the microparticle rheology also indicated a gel-like response near interfaces. This could indicate that interfacial gelation is also at play. Rheological measurements of other natural systems containing mucin or mucin-like proteins exhibit signatures of structuring at the air–water interface, like saliva[53] and lubricin.[65] Collectively, these results suggest that natural mucins may also exhibit gelation near interfaces.

Such interfacial-driven gelation may occur due to several effects. First, for solutions with amphiphilic molecules like all the examples cited above, localization at the air–water interface can permit alignment and thus enhanced bonding between H-bonding functional groups. However, our molecules have no hydrophobic groups and are not amphiphilic. Interfacial structuring was also observed for bovine serum albumin (BSA)[66] solutions; although BSA contains hydrophilic and hydrophobic groups, they are distributed throughout the protein and so it is not amphiphilic. Structuring of BSA at the air–water interface was confirmed with a DWR measurement, while a Newtonian response was observed away from the air–water interface using microfluidic rheometry. The authors conclude the BSA aggregates at the air–water interface,

but do not provide a physical or chemical explanation for the effect.

A second mechanism that could affect even purely hydrophilic molecules would be an increase in affinity for H-bonding at the air–water interface, which has been observed and attributed to the reduced dielectric screening between H-bonding groups (which normally is a strong effect in bulk water but which is reduced near the air–water interface) and associated charge redistribution.[67] A third possible mechanism arises from pH depression, which has been reported to be up to two units in the vicinity of the air–water interface.[68] A decrease in pH from neutral will reduce the net negative charge on mucin molecules and hence allow for easier intermolecular H-bonding.

Regardless of the mechanism, the effect of interfacial viscoelastic response leading to misinterpretation of cone- or parallel-plate rheometry has not been previously reported except for the case of amphiphilic molecules.[53,65,66]

2.3. Predicted Interfacial Microphysics by Kinetic Monte Carlo Simulations

To quantitatively understand the dynamics of these intermolecular associations between mucin chains under shear at the air–water interface, a mathematical model has been formulated, and kinetic Monte Carlo simulations have been run to test this model. Poly(Gal-Thr)$_{22}$ mucins are bottlebrush chains with a persistence length that exceeds their contour length, meaning that the backbone is highly rigid due to the steric constraints of the bulky sugar groups which decorate them combined with the short overall length of each synthetic mucin molecule (≈10 nm). This makes our mucins relatively rigid even when subjected to shear.[54] Alongside the backbone, there are multiple glycan sites, each of which can support multiple intermolecular H-bonds with neighboring mucins.[69] An expected net negative charge at neutral pH leads to net repulsion between mucin molecules and opposes the tendency to form H-bonds. Indeed, most literature expects intermolecular bonding in this pH range to be weak, explaining the lack of observed gelation in these studies.[45] However, as mentioned above, near the air–water interface, the pH may be suppressed,[68] and water-soluble molecules can show strongly enhanced H-bond strength.[67] Thus, even though the bulk structure is not crosslinked, the interfacial region can experience enhanced bonding and a cross-linked structure, as shown schematically in **Figure** 4a–c.

Based on our results and the literature described above, we develop a reduced-order toy model to understand how the response of an interfacial layer may influence the observed dynamics. As described further below, the model is designed to represent the behavior of molecules interacting via intermolecular H-bonds at the air–water interface[70] that contributes to the apparent yield stress[66] independent and uncoupled from the surrounding bulk, which behaves like a Newtonian fluid with particles moving in a Brownian fashion.[71–73] We consider the possibility of multiple intermolecular H-bonds, as this can enhance the degree of extension[74] and subsequently increase the time between complete association and complete dissociation of two chains under shear.[75]

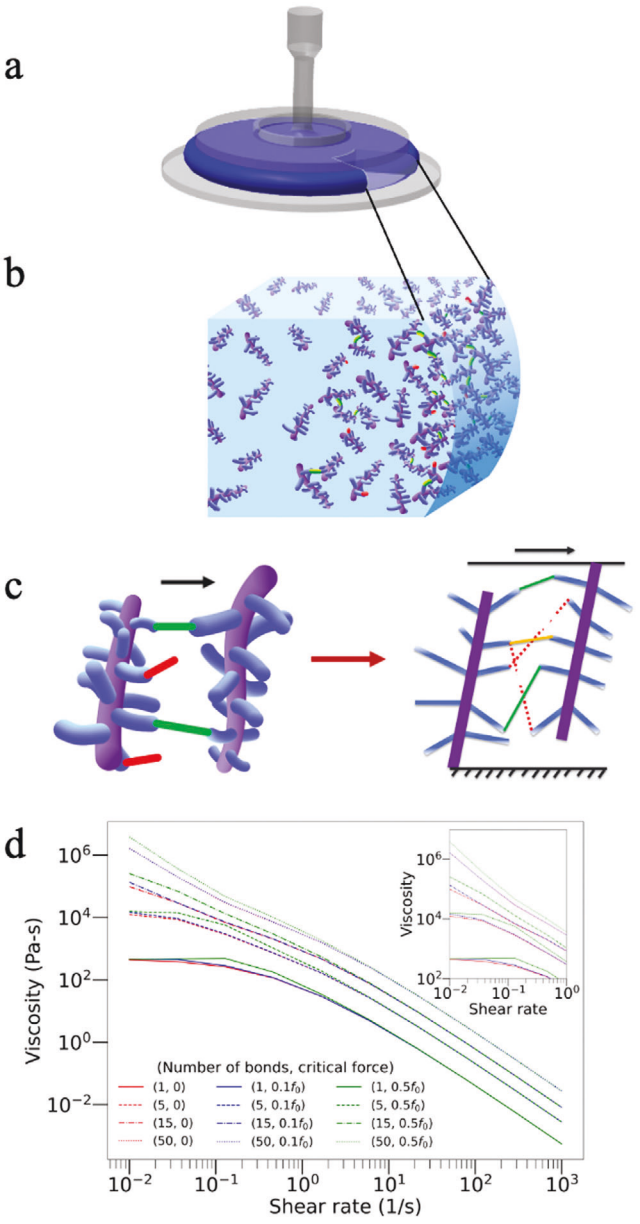

Figure 4. a) The cone-plate rheometer setup. b) The air–water interface. Mucins (purple backbone with blue glycan branches) are dissolved throughout the liquid, but an increased amount of bonding occurs between mucins near the air–water interface. Green lines indicate existing bonds, and red dashed lines indicate broken bonds. c) (left) A zoomed-in view of a pair of mucins near the air–water interface and (right) how two such mucins are treated in the reduced-order model used for understanding the dynamics of mucin chains under shear: one molecule attached to a fixed virtual surface is sheared past the other attached to a moving virtual surface; periodic boundary conditions (not indicated) are used to effectively represent one shear plane in a continuum. Green and red lines again indicate intact and broken bonds between chains; the yellow line indicates rebonding (i.e., where a site that had previously been bonded to a site on another molecule has broken and then bonded to another site on that molecule; this situation is explicitly considered in the model as discussed in Section S3 of the Supporting Information). d) Simulated flow curves at different critical forces and different bonding states from the computational model.

A schematic of the model is shown in Figure 4c (right), where there are two mucin chains, each with multiple bonding sites[76] with relative motion between the chains due to the flow resulting in the intermolecular bonds experiencing shear. With a single bond, the total energy is dissipated after complete debonding.[77] With multiple bonds between two chains, some bonds can break and reform before all bonds have been broken, leading to longer average times for complete debonding, resulting in a greater dissipation when all bonds have been broken. We model these as Markov chains, which are stochastic processes where each event depends on the event that occurred before. These Markov chains are then coupled with kMC simulations[78,79] to model the debonding of the intermolecular bonds between these chains under shear.

In this reduced order toy model, a single layer of molecules is considered. Uniform shear is imposed by having one molecule anchored to a virtual bottom layer that is fixed, and the other molecule anchored to a virtual top layer that shears past the bottom layer with a velocity V. Periodic boundary conditions in the shear direction are imposed. Thus, in the model the bonds are distributed like an annulus around the interface rather than through the bulk, where each pair of chains would locally be sheared with a different velocity. This simple setup is motivated by prior work showing such a model is effective in representing the rheological behavior of associating molecules subjected to uniform shear.[77] However, we go beyond the treatment in ref. [77] by 1) considering not just one but possibly multiple bonding sites for both molecules; 2) allowing different numbers of intermolecular bonds to exist between the molecules at any given time; and 3) considering the possibility that the debonding rate can depend on the amount of force that the bonds experience when stretched. As in ref. [77], the bonds stretch as the top layer moves past the bottom layer. Each set of bonds between chains can have a different and independent trajectory from all the others.

To simulate the dynamics of the model with N possible bonding sites between mucin chains, we assume that at low shear speeds, debonding and rebonding only occur when the bonds dislocate stochastically without completely debonding, which results in negligible dissipation. This is appropriate as the structure is the least perturbed under these conditions, and this is the region where the perceived apparent yield stress regime occurs. This makes the debonding rate force-independent until a certain force f_{cr} is reached. After this force is reached, we assume that the debonding becomes force-dependent. The force f_{cr} thus changes the rate of debonding to a piecewise function as,

$$k_{\text{off}} = \begin{cases} k_{\text{off}}; & F(Vt) < f_{\text{cr}} \\ k_{\text{off}} \exp\left(\frac{F(Vt) r_b}{k_B T}\right); & F(Vt) \geq f_{\text{cr}} \end{cases} \quad (1)$$

Thus, the dissipation varies with the shear speed in a force-independent fashion when the shear speeds are small, and eventually starts varying with the shear speed in a force-dependent fashion as the shear speed increases. The value of f_{cr} is not known, hence it has been varied in the KMC simulations to observe how a variation in the domain of a negligible dissipation rate translates to a stronger shear thinning response when transformed to viscosity (see Sections S4 and S5 of the Supporting Information). We use values for f_{cr} of 0, $0.1f_0$, and $0.5f_0$ where f_0 is chosen to be the ratio of $k_B T$ to the persistence length, i.e., the force scale in the worm-like chain model, which describes well the force-dependent stretching of relatively stiff, semi-flexible polymers like our mucin by modeling it as a continuous, flexible, isotropic rod.[80] The results are shown in Figure 4d.

From Figure 4d we see that the curves commonly show a shear thinning response across four decades of shear rates starting from approximately 10^0 s^{-1}. As well, as more bonds per molecules are considered, the Newtonian plateau observed at lower shear rates transforms such that the viscosity keeps increasing as the shear rate decreases, qualitatively replicating the apparent yield stress-like response seen in Figure 1a.

Furthermore, for one bond per mucin pair, the flow curves remain the same for all values of f_{cr}. As the number of bonds increase, the low shear plateau shifts to the left until it is outside the simulated range of shear rates, leaving the archetypical response of yield stress behavior. This qualitatively shows that the experimental flow sweeps can be replicated with computational methods probing the microphysics of an interfacial bonded layer.

The importance of f_{cr} becomes apparent at higher numbers of bonds. For 50 bonds per molecule, the low shear rate viscosity increases as the value of f_{cr} increases. This is because, for a higher f_{cr}, individual bonds have a larger range of shear speeds with negligible dissipation, which increases the domain for solid-like behavior, thus making the shear thinning response more apparent. The degree of qualitative agreement with the experimental results depends on the value of f_{cr} when as more bonding sites per molecule are considered. In other words, the system more clearly exhibits yield stress behavior when the value of f_{cr} is nonzero for intermediate numbers of bonding sites. For the maximum number of bonding sites considered (50 per molecules), even at $f_{\text{cr}} = 0$, the breaking of any bond does not redistribute enough force onto the remaining bonds to accelerate the debonding of the entire chain, thus causing yield stress behavior. This finding suggests that there are both multiple bonding sites per molecule (which is expected given the mucin's structure) and that the nature of the bonding involves a force-dependent debonding rate. The latter has been observed for the forced unfolding of single biomolecules including many proteins[81,82] as well as the debonding of complementary DNA strands,[83] demonstrating the intermolecular interactions between our synthetic mucins are similar in this regard to those found in natural mucins.

Additionally, we quantitatively compare the kMC results with the experimental viscosity measurements. Converting the viscosity derived from the kMC for 50 bonds and $f_{\text{cr}} = 0.5f_0$ at a low shear rate of 10^{-1} s^{-1} corresponding to a region one molecule thick gives a predicted viscosity of ≈0.07 Pa s (see Section S7 of Supporting Information). This viscosity is comparable in magnitude to the apparent bulk viscosity in the cone-plate, which ranges from 0.07to1 Pa s across different concentrations at a shear rate of 10^{-1} s^{-1} with the two lowest concentrations being close to the experimental noise floor of the instrument. More rigorous quantitative insights would require accounting for additional effects including the presence of a solvent, the non-specific interactions between mucins (van der Waals forces), and more than just two mucins as shown in the toy model. To guide material design for a vast array of mucosal structures, the microphysics must be generalized into larger scale approaches such as finite element

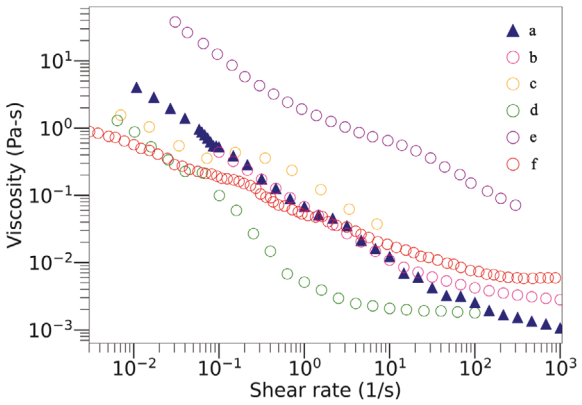

Figure 5. Flow sweeps at pH 4 of a) our synthetic mucin (at 10 mg mL^{-1}) compared with b) porcine gastric mucin solutions we prepared (at 10 mg mL^{-1}) c) partially purified porcine gastric mucin (at 50 mg mL^{-1})[18] d) porcine gastric mucin (at 10 mg mL^{-1})[45] e) porcine gastric mucin (at 15 mg mL^{-1}),[34] and f) porcine gastric mucin (at 10 mg mL^{-1}).[33]

modeling, which has not been explored here using this stochastic model. Though it is possible to further generalize the Markovian debonding process to account for multiple types of mucins and multiple independent processes coupled together, it does not add additional qualitative insight into modeling mucins under shear, which could be understood better with continuum models.

Regardless, the results of the simulations confirm that a model-based yielding of a bonded network with reasonable microphysics qualitatively explains and predict our experimental results, and moreover, has reasonable quantitative agreement with the experiments when applying the viscosity from the model to an interfacial layer (see Figure S7, Supporting Information).

2.4. Comparison to Natural Mucins and Further Discussion

We now compare our results to measurements of natural mucins in prior literature. Several studies have worked at pH 4 as it is physiologically relevant, and generally they report a modest increase in viscosity compared to neutral pH, attributed to some degree of gelation enabled by the reduced Coulombic repulsion[84] that glycan groups exhibit at pH 4.[45] Thus, we conducted further tests with our mucin dispersed in a buffered pH 4 solution while maintaining the concentration at 10 mg mL^{-1}. The resulting flow sweeps were nearly indistinguishable from those at neutral pH (see Figure S9, Supporting Information). Flow sweeps from cone-plate rheometry recorded with our synthetic mucin as well as porcine gastric mucin solutions we prepared using the same concentration, pH and surrounding buffer were overlayed with prior literature for natural mucin solutions with a pH of 4 as shown in **Figure 5**.[18,33,34,45]

All of the cited flow sweeps show shear thinning, viscosity values, and yield-stress behavior that are similar to ours (except for the larger magnitude viscosity seen for Celli et al.[34]), suggesting similar underlying microphysics despite the vast differences in molecular weight, and the substantial differences in the degree of associating groups, concentration, and amphiphilicity. However, the cited literature attributes the viscosity to bulk contributions. In contrast, we propose that a structured interface fully accounts for the attributes of the flow sweeps including the yield stress behavior. This suggests potential overlooked dynamics of mucin solution rheology, particularly regarding the role of the air–fluid interface versus the bulk, although it should be noted that natural mucuses are complex heterogenous mixtures, and these synthetic mucins are only intended to model the glycosylated domains of mucins.

As pointed out above, there is work suggesting interfacial structuring with mucins, including Jory et al.'s study of mucus simulants extracted from cultured human bronchial epithelium (HBE) cells. They reported a similar yield stress behavior while observing Newtonian behavior in microparticle tracking which can be explained by having a Newtonian bulk response. Another example is Celebioglu et al. who showed that bovine submaxillary mucins exhibit a gel-like interfacial response which they attribute to mucins segregating to the air–water interface.

For studies of mucus that employ experimental setups which effectively mitigate interfacial effects, such as falling ball viscometry[85] and particle tracking micro-rheology,[55] interpreting the results in terms of the bulk mucus behavior is justified. The latter study does report bulk gelation in a natural mucin system, MUC5AC at 10 mg mL^{-1}, with bulk gelation occurring at a low pH. To check for long term structural associations in our system, we conducted small amplitude oscillatory sweeps with 50 mg/mL Poly(Gal-Thr)$_{22}$ and observed that the storage and loss moduli rose over 3 orders of magnitude over a timespan of 2 h (see Figure S13b in the Supporting Information). Though this effect occurs, it cannot necessarily be attributed to bulk effects, as the interfacial layer thickening could lead to a similar response or even dominate over bulk structuring. This emphasizes the need for careful consideration of these nuances in experimentation, particularly interfacial rheological effects, when interpreting rheometry results. Failure to account for such effects could lead to misinterpretations of results and ensuing conclusions.

3. Conclusions

Synthetic mucin solutions of pure and highly monodisperse poly(Gal-Thr)$_{22}$ at concentrations of 0.1–10 mg mL^{-1} in DI water at neutral pH were studied. These molecules are close synthetic analogs to the highly glycosylated domains of natural mucins. The rheometry reveals yield stress behavior localized to the air–water interface, while the bulk response is Brownian. The interfacial yield stress response is attributed to inter-mucin H-bonding. We discuss two candidate mechanisms which could explain why there is a strong disparity in intermolecular associations between the bulk and the interface: strengthening of H-bonds due dielectric effects and pH reduction near the air–water interface, which reduces the Coulomb repulsion between isolated mucin molecules. An analytical model considering single or multiple bonds between mucins was developed and validated with kMC simulations. The kMC simulations can both qualitatively and reasonably quantitatively reproduce the interfacial rheological response when multiple bonding sites per molecule or a force-dependent debonding rate are assumed; both effects are consistent with the structure and bonding characteristics of our (and other) mucins.

These results provide a benchmark for understanding the spatial segregation of mucins to the air–water interface and its effect

on measured rheological behavior. This in turn can enable accurate microphysical interpretation of experimental rheometry, including separation of bulk and interfacial effects. The results, in combination with other literature studies of natural mucins, suggest that glycan-bearing domains can drive mucin segregation to air–water interfaces and may be important in understanding the first stages of gelation in mucus. There exists a growing interest in understanding the complex material properties of mucus, such as their transition from a solid-like structure at equilibrium to a fluid-like structure under shear. However, their rheological properties remain amongst the most difficult to quantify and model, and are often misinterpreted. To understand this complex topic, we have adopted the approach of creating a material whose structure seeks to emulate elements common to natural mucins. The ability of this synthetic material to reproduce the rheological properties of natural mucus validates this approach as a way to understand and recreate the fascinating rheology of mucus. We intend to explore the extensional rheology of these synthetic mucins to draw differences in extensional viscosities where the shear viscosities are comparable. We also intend to continue diversifying the structure of our synthetic mucins through various approaches like increasing the monomer chain lengths, adding cysteine links and even preparing block copolymers with these mucins, among other strategies. We plan on reporting those results in future publications that build directly on the methods and understanding developed in this work.

4. Experimental Section

Poly(Gal-Thr)$_{22}$ was prepared as previously reported,[23] and synthetic details and characterization are provided in Section S9 of the Supporting Information.

Preparation of Poly(Gal-Thr)$_{22}$ Solutions in DI Water: Mucin powder was stored in the freezer until use. Immediately prior to experiments, mucin powder was dispersed in deionized water. For the data at pH 4, a buffer consisting of 0.02 M HEPES free acid (0.4766g), 0.02 M sodium acetate trihydrate (0.16 g) and 0.02 M Bis-Tris (0.42 g) (all salts from Sigma Aldrich) were prepared in 100 mL DI water. This buffer was chosen because it is effective across a wide pH range.[37] 1 M HCl and 1 M NaOH were used to lower and elevate the pH respectively. Post dispersion, all solutions were sonicated for 30 min prior to starting experiments.

Preparation of Porcine Gastric Mucin Solutions in DI Water: Commercial porcine gastric mucin (type III, bound sialic acid 0.5–1.5%, partially purified powder, Sigma Aldrich) was bought and dispersed in the same buffer solution used for the synthetic mucins. A 10 mg mL^{-1} concentration of PGM was prepared at pH 4 to replicate the solvent conditions used for poly(Gal-Thr)$_{22}$.

Bulk Rheology: Bulk rheology tests were conducted on a DHR-3 (TA Instruments, New Castle, DE, USA) rheometer. Two different configurations for bulk rheology were used. The first was a 60 mm diameter, 1° anodized aluminum cone-plate, where a solvent trap was utilized to minimize sample evaporation. The solutions were pipetted in, the gap was lowered and the solutions were subjected to an initial high shear rate. Two replicates of these tests were performed with 900 µL of mucin solutions in DI water with concentrations 10, 5, 1, and 0.1 mg mL^{-1} and with 900 µL of 10 mg mL^{-1} mucin solutions in the buffer with pH 4 and pH 7.6. The tests included steady shear flow sweeps which measure viscosity as a function of shear rate from 0.1 to 1000 s^{-1}. Data were acquired with 6 points per decade of shear rate and a 30 s equilibration time between consecutive data points. Creep tests were also performed by imposing a constant shear stress and quantifying the accumulated strain for 500 s. The second rheometer geometry was a Couette cell with a Peltier rotor and standard cup concentric cylinder. All experiments were conducted at 25 °C. The Couette cell tests were flow sweeps performed with 16 mL of 10 mg mL^{-1} mucin solution in DI water. The shear rate was varied from 0.1 to 100 s^{-1}.

Interfacial Rheology: Interfacial rheology tests were also conducted with the DHR-3 rheometer by using a double-walled ring geometry made with platinum-iridium. These tests used 15 mL of 10 mg mL^{-1} mucin solution contained in a fluorocarbon trough.[38] Amplitude sweeps were conducted with a frequency of 0.1 Hz to observe the change in storage and loss moduli by an applied strain ranging from 0.001% to 10% with 6 points per decade, a sampling time of 15 s, and automatic termination when the oscillation strain exceeded 20%. Time-dependent changes in the shear modulus were also quantified with small amplitude oscillatory shear at a constant frequency of 0.1 Hz and a strain of 0.05%. These results were corrected with an iterative subphase correction iterative algorithm.[39]

Particle Tracking Micro-Rheology: Microparticle tracking measurements were performed using 1 µm diameter polystyrene fluorescent particles (F8811, Thermo Fisher Scientific Inc., Waltham, MA). Particles were suspended in square capillary tubes (8290-100, Wale Apparatus, Hellertown, PA) at a concentration of 1×10^{-4} wt% and imaged using 100x oil immersion lens and an sCMOS camera (Prime-95B, Photometrics, Tucson, AZ) with 1200×1200 pixel field of view and 80.53 fps. The fluorescent particles were excited with 480 nm laser and emission isolated with 535±35 nm bandpass filter. The image sequences were analyzed using TrackPy, an open source python package for particle tracking studies.

Supporting Information

Supporting Information is available from the Wiley Online Library or from the author.

Acknowledgements

This work was supported by National Science Foundation (NSF) through the grant DMR 2212139 to A.B.B. and grant DMR 2212162 to R.W.C. and P.K.P.; the NSF through grant TI 2304237 to M.A.L., A.B.B., and F.M.K, and the U.S. Air Force Office of Scientific Research through grants FA9550-23-2-0230 and FA9550-18-1-0142 to A.B.B. and a Llewellyn Fellowship from CUNY (M.A.L.). The authors acknowledge Dr. Paulo Arratia for the use of the rheometer which is part of the NSF Major Instrumentation Award NSF-MRI-1920156. The authors acknowledge the use of facilities supported by the Laboratory for Research on the Structure of Matter and the NSF through the University of Pennsylvania Materials research Science and Engineering Center (MRSEC) DMR-2309043. This work was carried out in part at the Singh Center for Nanotechnology, which is supported by the NSF National Nanotechnology Coordinated Infrastructure Program under grant NNCI-2025608.

Conflict of Interest

Co-authors Adam B. Braunschweig Manuel A. Lema, and Farhana M. Khan are cofounders of Nomi Materials Corp., which seeks to commercialize synthetic mucins.

Data Availability Statement

The data that support the findings of this study are available from the corresponding author upon reasonable request.

Keywords

biomimetic, biopolymer, gelation, mucus, rheology, synthetic mucins

Received: January 23, 2025
Published online: February 10, 2025

[1] A. R. Cerullo, T. Y. Lai, B. Allam, A. Baer, W. J. P. Barnes, Z. Barrientos, D. D. Deheyn, D. S. Fudge, J. Gould, M. J. Harrington, M. Holford, C.-S. Hung, G. Jain, G. Mayer, M. Medina, J. Monge-Nájera, T. Napolitano, E. P. Espinosa, S. Schmidt, E. M. Thompson, A. B. Braunschweig, *ACS Biomater. Sci. Eng.* **2020**, *6*, 5377.
[2] M. M. France, J. R. Turner, *J. Cell Sci.* **2017**, *130*, 307.
[3] G. Petrou, T. Crouzier, *Biomater. Sci.* **2018**, *6*, 2282.
[4] A. M. Smith, *Integr. Comp. Biol.* **2002**, *42*, 1164.
[5] L. Böni, P. Fischer, L. Böcker, S. Kuster, P. A. Rühs, *Sci. Rep.* **2016**, *6*, 30371.
[6] B. Chan, N. J. Balmforth, A. E. Hosoi, *Phys. Fluids* **2005**, *17*, 113101.
[7] T. Deng, D. Gao, X. Song, Z. Zhou, L. Zhou, M. Tao, Z. Jiang, L. Yang, L. Luo, A. Zhou, L. Hu, H. Qin, M. Wu, *Nat. Commun.* **2023**, *14*, 396.
[8] A. Kobayashi, I. Yamamoto, T. Aoyama, *Tribol. Ser.* **2003**, *41*, 429.
[9] A. R. Cerullo, M. B. McDermott, L. E. Pepi, Z.-L. Liu, D. Barry, S. Zhang, X. Yang, X. Chen, P. Azadi, M. Holford, A. B. Braunschweig, *Nat. Commun.* **2023**, *14*, 5361.
[10] L. E. Wallace, M. Liu, F. J. M. Van Kuppeveld, E. De Vries, C. A. M. De Haan, *Trends Microbiol.* **2021**, *29*, 983.
[11] D. Kavishvar, A. Ramachandran, *Adv. Colloid Interface Sci.* **2023**, *322*, 103049.
[12] C. B. Morrison, M. R. Markovetz, C. Ehre, *Pediatr. Pulmonol.* **2019**, *54*, S84.
[13] M. Yazdani, K. B. P. Elgstøen, H. Rootwelt, A. Shahdadfar, Ø. A. Utheim, T. P. Utheim, *Int. J. Mol. Sci.* **2019**, *20*, 3755.
[14] R. Bansil, B. S. Turner, *Curr. Opin. Colloid Interface Sci.* **2006**, *11*, 164.
[15] A. Curnutt, K. Smith, E. Darrow, K. B. Walters, E. S. Vasquez, S. Kundu, in AJKFluids2019: Fluid Measurement and Instrumentation; Micro and Nano Fluid Dynamics, Vol. *4*, American Society of Mechanical Engineers (ASME), New York City **2019**, p. 382, https://asmedigitalcollection.asme.org/FEDSM/proceedings/AJKFluids2019/59070/V004T06A016/1069383.
[16] M. Marczynski, K. Jiang, M. Blakeley, V. Srivastava, F. Vilaplana, T. Crouzier, O. Lieleg, *Biomacromolecules* **2021**, *22*, 1600.
[17] D. I. Pedro, D. T. Nguyen, J. G. Rosa, N. Diodati, J. Kim, J. I. Bowman, R. A. Olson, J. M. Urueña, B. S. Sumerlin, W. G. Sawyer, *Tribol. Lett.* **2021**, *69*, 155.
[18] J. Caicedo, J. E. Perilla, *Ing. Invest.* **2015**, *35*, 43.
[19] C. E. Wagner, M. Krupkin, K. B. Smith-Dupont, C. M. Wu, N. A. Bustos, J. Witten, K. Ribbeck, *Biomacromolecules* **2023**, *24*, 628.
[20] M. Jory, D. Donnarumma, C. Blanc, K. Bellouma, A. Fort, I. Vachier, L. Casanellas, A. Bourdin, G. Massiera, *Interface Focus* **2022**, *12*, 20220028.
[21] B. Demouveaux, V. Gouyer, F. Gottrand, T. Narita, J.-L. Desseyn, *Adv. Colloid Interface Sci.* **2018**, *252*, 69.
[22] T. A. Gerken, *Crit. Rev. Oral Biol. Med.* **1993**, *4*, 261.
[23] M. A. Lema, I. B. Nava-Medina, A. R. Cerullo, R. Abdelaziz, S. M. Jimenez, J. B. Geldner, M. Abdelhamid, C.-S. Kwan, L. Kharlamb, M. C. Neary, A. B. Braunschweig, *Macromolecules* **2022**, *55*, 4710.
[24] R. E. Detwiler, J. R. Kramer, *Curr. Opin. Solid State Mater. Sci.* **2022**, *26*, 101031.
[25] S. Laneri, R. D. Lorenzo, A. Sacchi, I. Dini, *Nat. Prod. Commun.* **2019**, *14*, 1934578X19868606.
[26] Z. S. Clauss, J. R. Kramer, *Adv. Drug Delivery Rev.* **2021**, *169*, 152.
[27] C. V. Duffy, L. David, T. Crouzier, *Acta Biomater.* **2015**, *20*, 51.
[28] K. Jiang, H. Yan, C. Rickert, M. Marczynski, K. Sixtensson, F. Vilaplana, O. Lieleg, T. Crouzier, *Adv. Funct. Mater.* **2021**, *31*, 2008428.
[29] H. Yan, C. Seignez, M. Hjorth, B. Winkeljann, M. Blakeley, O. Lieleg, M. Phillipson, T. Crouzier, *Adv. Funct. Mater.* **2019**, *29*, 1902581.
[30] W. Lin, J. Klein, *Adv. Mater.* **2021**, *33*, 2005513.
[31] D. Morniroli, A. Consales, B. L. Crippa, G. Vizzari, F. Ceroni, J. Cerasani, L. Colombo, F. Mosca, M. L. Giannì, *Nutrients* **2021**, *13*, 694.
[32] T. A. Waigh, A. Papagiannopoulos, A. Voice, R. Bansil, A. P. Unwin, C. D. Dewhurst, B. Turner, N. Afdhal, *Langmuir* **2002**, *18*, 7188.
[33] A. Maleki, G. Lafitte, A.-L. Kjøniksen, K. Thuresson, B. Nyström, *Carbohydr. Res.* **2008**, *343*, 328.
[34] J. P. Celli, B. S. Turner, N. H. Afdhal, R. H. Ewoldt, G. H. McKinley, R. Bansil, S. Erramilli, *Biomacromolecules* **2007**, *8*, 1580.
[35] C. Kwan, A. R. Cerullo, A. B. Braunschweig, *ChemPlusChem* **2020**, *85*, 2704.
[36] M. J. Caulfield, G. G. Qiao, D. H. Solomon, *Chem. Rev.* **2002**, *102*, 3067.
[37] M. N. Zhou, C. S. Delaveris, J. R. Kramer, J. A. Kenkel, E. G. Engleman, C. R. Bertozzi, *Angew. Chem., Int. Ed. Engl.* **2018**, *57*, 3137.
[38] J. R. Kramer, B. Onoa, C. Bustamante, C. R. Bertozzi, *Proc. Natl. Acad. Sci. USA* **2015**, *112*, 12574.
[39] O. Lieleg, K. Ribbeck, *Trends Cell Biol.* **2011**, *21*, 543.
[40] V. Croce, T. Cosgrove, C. A. Dreiss, S. King, G. Maitland, T. Hughes, *Langmuir* **2005**, *21*, 6762.
[41] I. Pincus, A. Rodger, J. R Prakash, *J. Rheol.* **2023**, *67*, 373.
[42] J. Sepulveda, A. Montillet, D. D. Valle, T. Amiar, H. Ranchon, C. Loisel, A. Riaublanc, *Appl. Rheol.* **2021**, *31*, 24.
[43] E. K. Hobbie, *Rheol. Acta* **2010**, *49*, 323.
[44] M. Bercea, P. Navard, *Macromolecules* **2000**, *33*, 6011.
[45] A. Curnutt, K. Smith, E. Darrow, K. B. Walters, *Sci. Rep.* **2020**, *10*, 8760.
[46] A. Giboreau, G. Cuvelier, B. Launay, *J. Texture Stud.* **1994**, *25*, 119.
[47] Q. D. Nguyen, D. V. Boger, *Annu. Rev. Fluid Mech.* **2003**, *24*, 47.
[48] A. Z. Nelson, K. S. Schweizer, B. M. Rauzan, R. G. Nuzzo, J. Vermant, R. H. Ewoldt, *Curr. Opin. Solid State Mater. Sci.* **2019**, *23*, 100758.
[49] R. Ewoldt, C. Clasen, A. E. Hosoi, G. H. McKinley, *Soft Matter* **2007**, *3*, 634.
[50] J. P. Celli, B. S. Turner, N. H. Afdhal, S. Keates, I. Ghiran, C. P. Kelly, R. H. Ewoldt, G. H. McKinley, P. So, S. Erramilli, R. Bansil, *Proc. Natl. Acad. Sci. USA* **2009**, *106*, 14321.
[51] X. Cao, R. Bansil, K. R. Bhaskar, B. S. Turner, J. T. LaMont, N. Niu, N. H. Afdhal, *Biophys. J.* **1999**, *76*, 1250.
[52] G. Javitt, L. Khmelnitsky, L. Albert, L. S. Bigman, N. Elad, D. Morgenstern, T. Ilani, Y. Levy, R. Diskin, D. Fass, *Cell* **2020**, *183*, 717.
[53] D. Rossetti, G. E. Yakubov, J. R. Stokes, A.-M. Williamson, G. G. Fuller, *Food Hydrocolloids* **2008**, *22*, 1068.
[54] B. Zappone, N. J. Patil, J. B. Madsen, K. I. Pakkanen, S. Lee, *Langmuir* **2015**, *31*, 4524.
[55] C. E. Wagner, B. S. Turner, M. Rubinstein, G. H. McKinley, K. Ribbeck, *Biomacromolecules* **2017**, *18*, 3654.
[56] S. Vandebril, A. Franck, G. G. Fuller, P. Moldenaers, J. Vermant, *Rheol. Acta* **2010**, *49*, 131.
[57] D. Renggli, A. Alicke, R. H. Ewoldt, J. Vermant, *J. Rheol.* **2020**, *64*, 141.
[58] R. H. Alasfar, S. Ahzi, N. Barth, V. Kochkodan, M. Khraisheh, M. Koç, *Polymers* **2022**, *14*, 360.
[59] Y. El Bitouri, *Eng* **2023**, *4*, 1891.
[60] P. Moller, A. Fall, V. Chikkadi, D. Derks, D. Bonn, *Philos. Trans. R. Soc., A* **2009**, *367*, 5139.
[61] M. W. Denny, J. M. Gosline, *J. Exp. Biol.* **1980**, *88*, 375.
[62] M. Denny, *Nature* **1980**, *285*, 160.
[63] F. Caton, C. Baravian, *Rheol. Acta* **2008**, *47*, 601.
[64] H. Y. Çelebioğlu, J. Kmiecik-Palczewska, S. Lee, I. S. Chronakis, *Int. J. Biol. Macromol.* **2017**, *102*, 857.
[65] L. Martin-Alarcon, A. Govedarica, R. H. Ewoldt, S. L. Bryant, G. D. Jay, T. A. Schmidt, M. Trifkovic, *Small* **2024**, *20*, 2306207.
[66] V. Sharma, A. Jaishankar, Y.-C. Wang, G. H. McKinley, *Soft Matter* **2011**, *7*, 5150.
[67] K. Ariga, *Phys. Chem. Chem. Phys.* **2020**, *22*, 24856.
[68] H. Yang, Y. Imanishi, A. Harata, *Anal. Sci.* **2015**, *31*, 1005.
[69] M. M. Deshmukh, L. J. Bartolotti, S. R. Gadre, *J. Phys. Chem. A* **2008**, *112*, 312.
[70] T. W. Patapoff, O. Esue, *Pharm. Dev. Technol.* **2009**, *14*, 659.

[71] G. Drazer, J. Koplik, B. Khusid, A. Acrivos, *J. Fluid Mech.* **2002**, *460*, 307.
[72] J. G. Hernández Cifre, R. Pamies, A.-L. Kjøniksen, K. D. Knudsen, B. Nyström, J. García de la Torre, *J. Non-Newtonian Fluid Mech.* **2007**, *146*, 3.
[73] G. Bossis, J. F. Brady, *J. Chem. Phys.* **1987**, *87*, 5437.
[74] A. N. Round, M. Berry, T. J. McMaster, A. P. Corfield, M. J. Miles, *J. Struct. Biol.* **2004**, *145*, 246.
[75] A. Erbaş, D. Horinek, R. R. Netz, *J. Am. Chem. Soc.* **2012**, *134*, 623.
[76] S. Ge, M. Tress, K. Xing, P.-F. Cao, T. Saito, A. P. Sokolov, *Soft Matter* **2020**, *16*, 390.
[77] T. Leadbetter, A. Seiphoori, C. Reina, P. K. Purohit, *J. Mech. Phys. Solids* **2022**, *158*, 104660.
[78] N. Li, A. Nikoubashman, A. Z. Panagiotopoulos, *J. Chem. Phys.* **2018**, *149*, 084904.
[79] R. Ran, S. Pradeep, S. K. Acharige, B. C. Blackwell, C. Kammer, D. J. Jerolmack, P. E. Arratia, *J. Rheol.* **2023**, *67*, 241.
[80] J. F. Marko, E. D. Siggia, *Macromolecules* **1995**, *28*, 8759.
[81] M. Rief, H. Grubmüller, *ChemPhysChem* **2002**, *3*, 255.
[82] F. Kienberger, A. Ebner, H. J. Gruber, P. Hinterdorfer, *Acc. Chem. Res.* **2006**, *39*, 29.
[83] I. Schumakovitch, W. Grange, T. Strunz, P. Bertoncini, H.-J. Güntherodt, M. Hegner, *Biophys. J.* **2002**, *82*, 517.
[84] N. M. Casellas, L. Albertazzi, S. Pujals, T. Torres, M. García-Iglesias, *Chem. - Eur. J.* **2021**, *27*, 11056.
[85] B. F. Smith, J. A. Peetermans, T. Tanaka, J. T. LaMont, *Gastroenterology* **1989**, *97*, 179.

